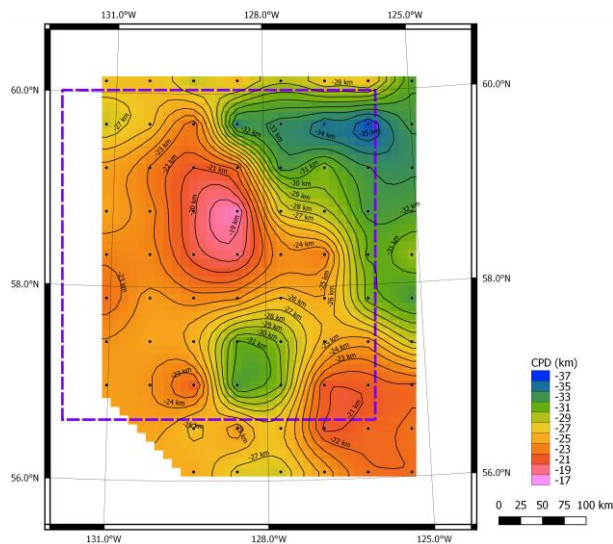




## Curie Point Depth Mapping Pilot Study in Northwest British Columbia

### Geoscience BC Report 2016-14



By:

Jeff Witter, Mira Geoscience Ltd.

and

Craig Miller, Simon Fraser University/Mira Geoscience MITACS scholar

409 Granville Street, Suite 512B, Vancouver, BC, Canada V6C 1T2

September 2016

---

## Executive Summary

We performed a Curie point depth (CPD) mapping pilot study over a ~350 km x ~350 km region of northwestern British Columbia. CPD mapping utilizes regional-scale magnetic survey data to map the depth in the Earth's crust to the Curie point temperature (~580 °C) where magnetization disappears. When used in combination with other data (such as heat flow) it can serve as a regional scale geothermal prospecting tool. For example, regions with shallow Curie point depths are expected to have higher heat flow and a higher likelihood of accessible geothermal energy resources. We chose the northwest corner of British Columbia for this pilot study because of: available public domain magnetic data, evidence for elevated heat flow, presence of Holocene volcanoes and hot springs, and evidence for localized crustal extension. Within the study area, the calculated CPD values have the range 18 – 36 km. In general, the deepest CPD values (> 30 km) lie in the northeastern part of the study area and coincide with the North American craton. The southeast corner and most of the western half of the study area have relatively shallow CPD values of 18 – 24 km. CPD estimates under the Holocene volcanic centres (23-24 km) within the study area are much deeper than typical CPD values below active subduction zone volcanoes (i.e. < 10 km). There appears to be no consistent correlation between CPD value and hot spring locations. Although heat flow data from existing wells are sparse, regions of higher heat flow in the study area generally correspond to zones with shallower CPD and vice versa. In this study, we used the shallow CPD values of 18 – 24 km to calculate heat flow values of 75 – 101 mW/m<sup>2</sup>. These heat flow values are in general agreement with the range of measured heat flow data in the western half and southeast corner of the study area. Such elevated heat flow is typical of electricity-grade geothermal regions such as the Great Basin of the USA. This pilot study has demonstrated that deep crustal temperatures and heat flow can be estimated for British Columbia using the CPD methodology described. Nearly the entire province is covered by public domain magnetic survey data. Therefore, CPD analysis can be applied province-wide. A CPD/heat flow map of British Columbia would complement the existing heat flow data for the province and could help guide future geothermal exploration programs towards prospective areas.

## Table of Contents

1. Introduction .....	5
2. Data Used .....	8
3. Methodology .....	10
4. Results .....	13
5. Discussion.....	16
6. Conclusions .....	23
7. Recommendations .....	24
8. List of Deliverables.....	25
References.....	26
Appendix 1: List of $Z_o$ , $Z_t$ , and $Z_b$ values.....	29

## List of Figures

Figure 1. Public domain magnetic data for British Columbia .....	6
Figure 2. Heat flow map of British Columbia. ....	7
Figure 3. Center point locations for the windows used to calculate Curie point depth.....	9
Figure 4. Example plots of magnetic power spectrum vs. wavenumber.....	12
Figure 5. Curie point depth map for northwestern BC. ....	14
Figure 6. Curie point depth map underlain by magnetic data. ....	15
Figure 7. Curie point depth map and the locations of hot springs and volcanoes .....	17
Figure 8. Existing heat flow map and the Curie point depth map .....	18
Figure 9. Regional geologic terrane map and the Curie point depth map .....	20

## 1. Introduction

This report presents the results of a pilot study to perform Curie Point Depth (CPD) mapping over a ~350 km x ~350 km region of northwestern British Columbia. The results of this pilot study are compared at a high-level with the BC heat flow map, known volcanism, hot springs, and regional geology to assess whether a province-wide CPD mapping exercise may be warranted.

CPD mapping is a methodology, originally developed in the 1970's, which utilizes regional-scale magnetic survey data to map the depth in the Earth's crust to the Curie point temperature (~580 °C) where magnetization in rocks disappears. CPD mapping has been used in combination with other methods (such as heat flow measurements) in many parts of the world as a regional scale geothermal prospecting tool. One advantage of CPD mapping is it provides information on crustal temperatures at depths not accessible by other means (Okubo et al., 1985). Examples of CPD studies include: the USA (e.g. Bouligand et al., 2009), Japan (e.g. Okubo et al., 1985; Okubo et al., 1989; Tanaka et al., 1999), Turkey (e.g. Aydin et al., 2005; Bilim et al., 2016), Mexico (e.g. Espinosa-Cardena and Campos-Enriquez, 2008; Manea and Manea, 2011), Afghanistan (Saibi et al., 2015), and Taiwan (Hseih et al., 2014). Regions found to have shallow Curie point depths are expected to have higher heat flow, higher average temperature gradient, and, therefore, a higher likelihood of geothermal energy resources accessible via drilling. The CPD mapping method is particularly suited for British Columbia because of the availability of public domain magnetic survey data that covers the majority of the province (Figure 1). CPD mapping has the potential to be a valuable complement to the existing heat flow map of BC which has gaps due to a lack of public domain downhole temperature data for much of the province (Figure 2). The northwest corner of British Columbia was chosen for this pilot study for a number of reasons: evidence for elevated heat flow (Grasby et al., 2012), presence of Holocene volcanoes and hot springs, and evidence for localized crustal extension (e.g. Edwards and Russell, 1999).

In this report, we briefly describe the data and methodology used for CPD mapping. The CPD results are then compared spatially, in a generalized manner, with both existing

heat flow estimates and the locations of Holocene volcanoes and hot springs. A detailed analysis of possible correlations between the CPD results and geoscience features is beyond the scope of this study. We conclude this report with a brief discussion of the CPD results in light of regional geology and geothermal energy potential in northwest BC.

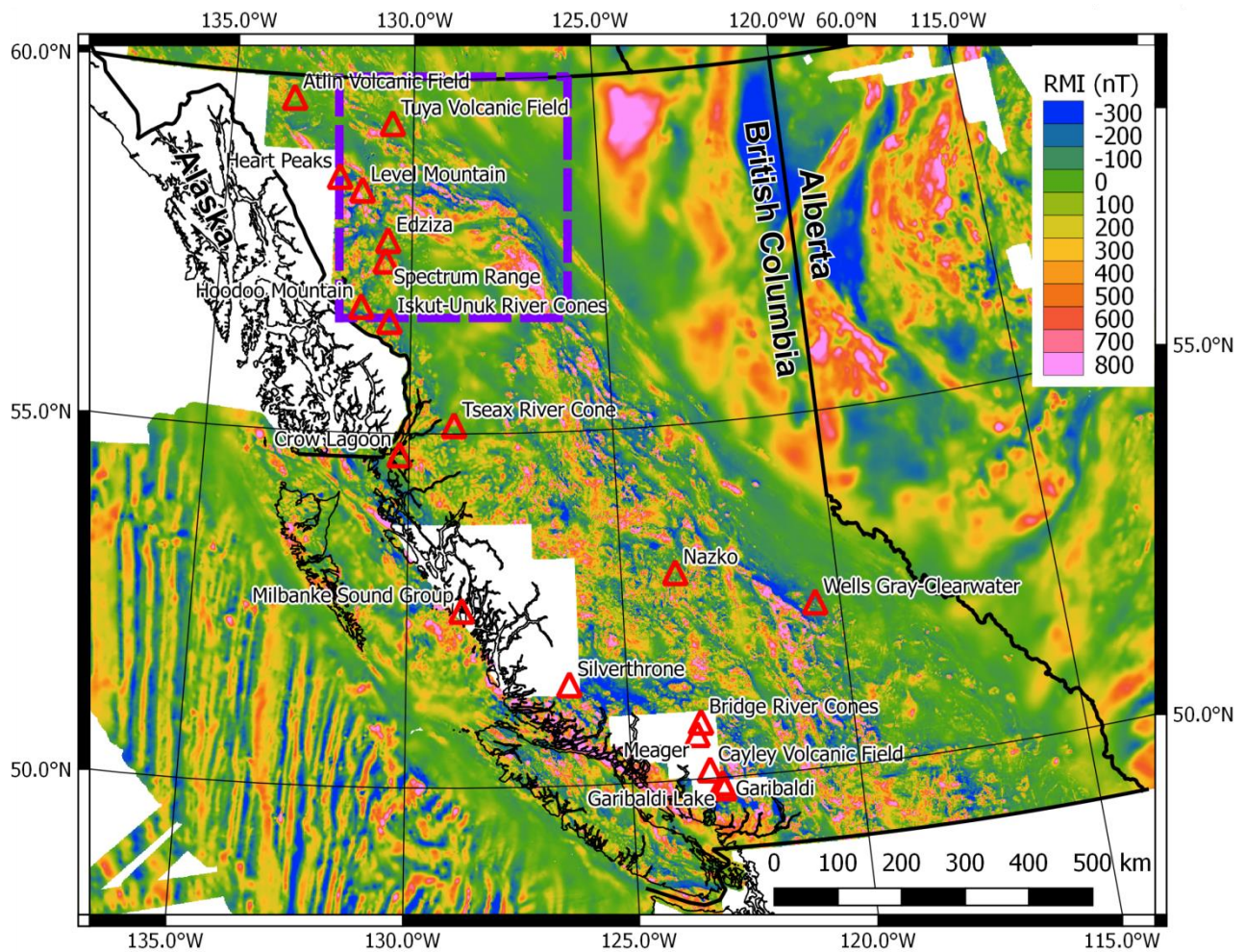


**Figure 1.** Map showing the distribution of public domain magnetic data for British Columbia as Residual Magnetic Intensity (RMI) in units of nanoTesla (nT). Warm colours represent magnetic highs and cool colours, magnetic lows. Isolated white areas in the westernmost portions of the province have no magnetic data. Holocene volcanoes are shown as red triangles (Smithsonian Institution Global Volcanism Program, 2016). The study area is outlined by the purple box. Map is in UTM NAD83 zone 9.

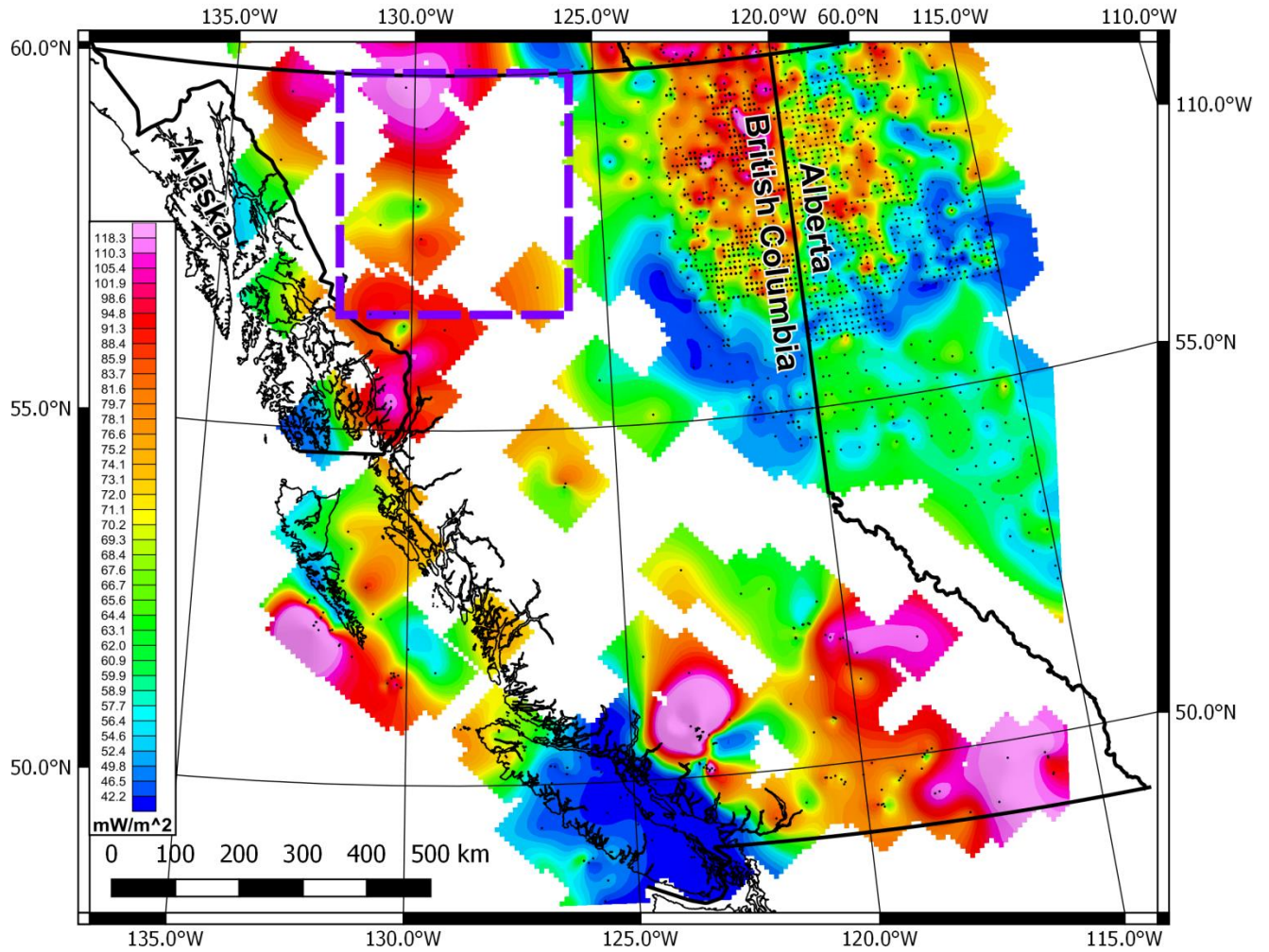


**Figure 2.** Heat flow map of British Columbia from Geoscience BC (2016). Heat flow estimates (derived from well data) for the northwest portion of BC covered by this study range from 68 – 118 mW/m<sup>2</sup>. The study area is outlined by the purple box. Map is in UTM NAD83 zone 9.

## 2. Data Used

Information on the hot springs of northwest BC was obtained from the GIS data files associated with Geoscience BC report 2016-07 “Direct-Use Geothermal Resources in British Columbia” (<http://www.geosciencebc.com/s/Report2016-07.asp>). Discharge temperatures of the hot springs within the study area have the range 13 – 52 °C; however, for several hot springs, temperature is not known.

Locations of Holocene volcanoes of northwest BC were obtained from the Smithsonian Institution Global Volcanism Program (<http://volcano.si.edu/>). These locations are similar to a broader Neogene – Quaternary list of volcanic centres described in Edwards and Russell (2000). Holocene volcanoes are those which have had an eruption in the last ~10,000 years.

Magnetic data used in this pilot study were obtained from the Natural Resources Canada Geoscience Data Repository for Geophysical Data (<http://gdr.agg.nrcan.gc.ca/>). These data are residual total field magnetic data that have been compiled from multiple airborne magnetic surveys. The data have been computationally-draped to an altitude of 305 m and gridded with a 200 m cell size.

The portion of northwest BC chosen for this pilot study is rectangular in shape and extends from the Yukon/BC border in the north to ~30 km south of Bob Quinn Lake (Figure 3). It also extends from Liard River Hot Springs in the east to ~100 km west of Dease Lake. The exact dimensions of the pilot study area are: 360 km (E-W) x 380 km (N-S). The magnetic data used in this study extend 50 – 100 km outside the pilot study boundary on the northern, southern, and eastern borders so that CPD contours can be drawn slightly beyond the edge of the study area (see Figure 3). This was not possible on the western side of the pilot study area because public domain magnetic data is not yet available for this area.

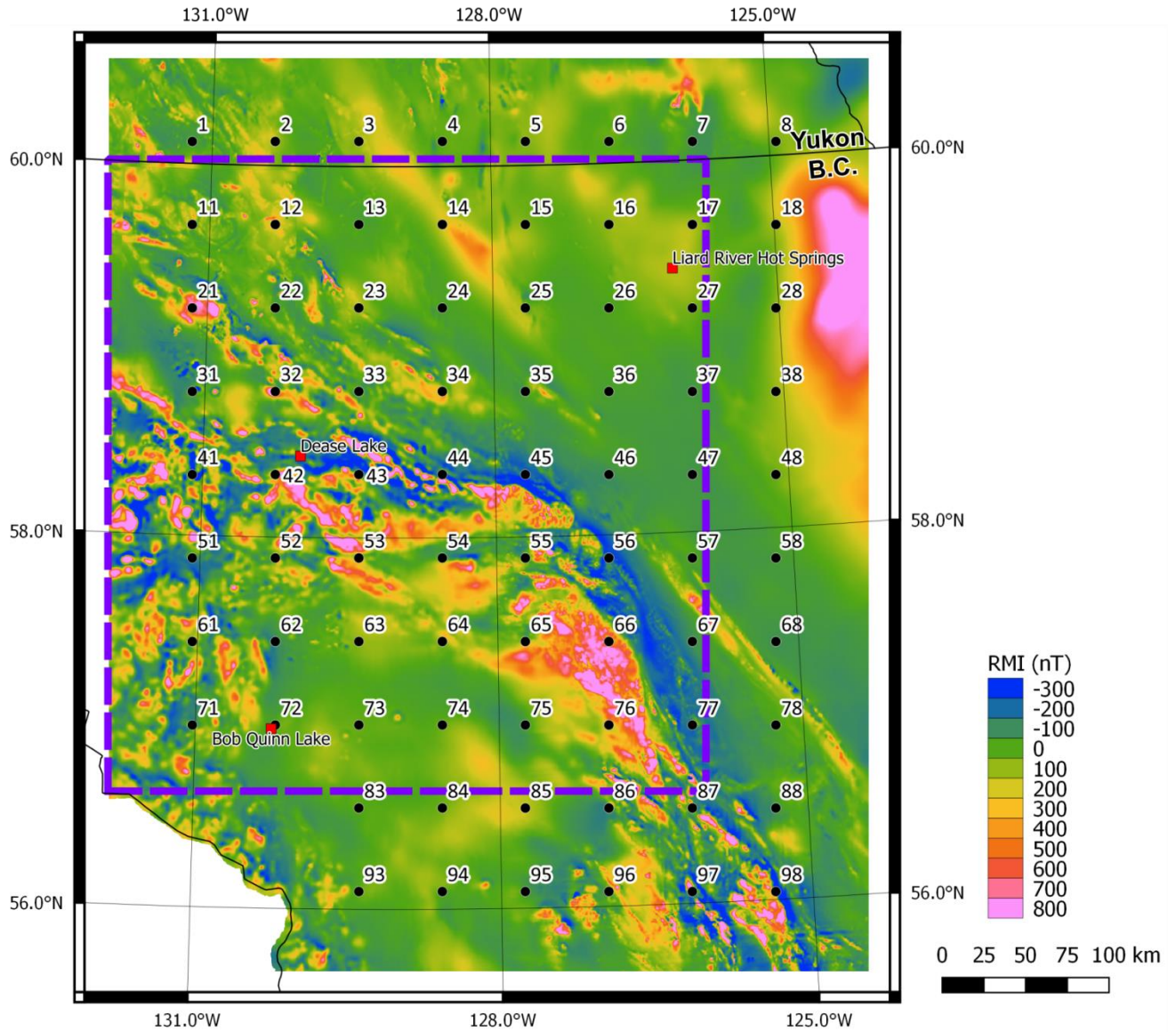


**Figure 3.** Map showing the study area (purple box) and the center point locations of the 76 windows used to calculate CPD. The numbers for the window centers are not consecutive. The residual magnetic field data used in the study is shown in the background in units of nanoTesla. Map is in UTM NAD83 zone 9.

### 3. Methodology

The idea of using magnetic data to estimate the depth to the Curie point arose in the mid-20<sup>th</sup> century (Vacquier and Affleck, 1941). But it wasn't until the topic was revisited in the 1970-80's that a sound methodology was developed (Spector and Grant, 1970; Bhattacharyya et al., 1975; Shuey et al., 1977; Connard et al., 1983; Okubo et al., 1985; Blakely, 1988; Okubo et al., 1989). Further refinements to the method in the 1990's (e.g. Tanaka et al., 1999) resulted in the CPD mapping technique that we employ here for northwest BC.

The CPD mapping method assumes that long wavelength magnetic anomalies are related to large-size, randomly magnetized sources within the Earth's crust that extend to depths of a few to tens of kilometres. The bottoms of these magnetic sources are assumed to correspond to the ~580 °C Curie Point temperature. Each CPD value is calculated at the centre of a square magnetic data "window" that has dimensions large enough to contain the long wavelength information required to estimate the CPD at any given location. Calculation windows are commonly overlapped with adjacent windows by ~50% to increase the density of CPD estimates and to enhance the spatial continuity of the generated CPD map. The depth to the base of the magnetic source (i.e. the Curie point depth) is calculated in four steps (Tanaka et al., 1999):

1. Calculate the radially averaged power spectrum of the magnetic data in each window
2. Estimate the depth to the top of the magnetic source ( $Z_t$ ) using the high wave number portion of the magnetic anomaly power spectra
3. Estimate the depth to the centroid of the magnetic source ( $Z_o$ ) using a lower wave number portion of the magnetic anomaly power spectra
4. Calculate the depth to the base of the magnetic source ( $Z_b$ ) using  $Z_b = 2Z_o - Z_t$ .  
The value of  $Z_b$  is the CPD.

The magnetic data obtained for the study area were divided into 76 square "windows" that each measure 100 km x 100 km in size. Similar to other CPD studies, the windows were created such that they overlap adjacent windows by 50% (Figure 3). There is some discussion in the literature regarding how large the CPD windows must be to

incorporate enough long wavelength magnetic signal. As a test, we ran the CPD calculations using a 200 km x 200 km window size (18 CPD values) and the results were similar to those obtained with 100 km windows. From this, we conclude that the 100 km windows sufficiently capture the long wavelength information for our CPD calculations. In addition, the majority of the power spectra show the characteristic roll off at low wavenumbers, indicating that the base of magnetization has been reached.

For each window, the power spectra was calculated using the `grdfft` function in the Generic Mapping Tools software (<http://gmt.soest.hawaii.edu/>) and then plotted vs. wavenumber according to Tanaka et al. (1999). An example from window 23 is shown in Figure 4. The depth to top ( $Z_t$ ) and depth to centroid ( $Z_o$ ) of the magnetic source were calculated from the slopes of the lines in the power spectra graphs.

In the scientific literature on CPD mapping, there is no specific and defined wavenumber range for calculating  $Z_o$  and  $Z_t$ . We experimented with different high and low wavenumber ranges to calculate slopes for determining  $Z_o$  and  $Z_t$  in order to assess the sensitivity of our choices. We found that varying the selected wavenumber range by reasonable amounts changed the  $Z_o$ ,  $Z_t$ , and  $Z_b$  values by less than 10%. For consistency, we used the same high and low wavenumber ranges for all windows to calculate the slopes for  $Z_t$  and  $Z_o$ . These wavenumber ranges are: 0.023 – 0.067 ( $Z_t$ ) and 0.0007 – 0.041 ( $Z_o$ ).

Limitations of the CPD mapping method include the following. First, long wavelength noise in the magnetic field may be present and can be challenging to detect, especially in a compilation of magnetic survey data such as the one used here. Such noise may cause CPD calculations to be in error (Blakely, 1988). Second, the method of Tanaka et al. (1999) assumes that the Earth's crust is randomly magnetized, but this assumption may not always be valid (Bouligand et al., 2009). Third, the magnetic source base depth ( $Z_b$ ) may not represent the Curie point depth but instead could simply be a geologic contact between magnetic and non-magnetic rocks. If this is the case, the calculated CPD may be unrelated to crustal temperatures and the Curie point temperature may actually lie at greater depths. Despite these limitations, a comparison of many CPD studies by Ravat et al. (2007) showed that most CPD estimates are likely accurate to

within a few kilometres. For a more detailed explanation of the methodology utilized in this study see Tanaka et al. (1999) and references therein.

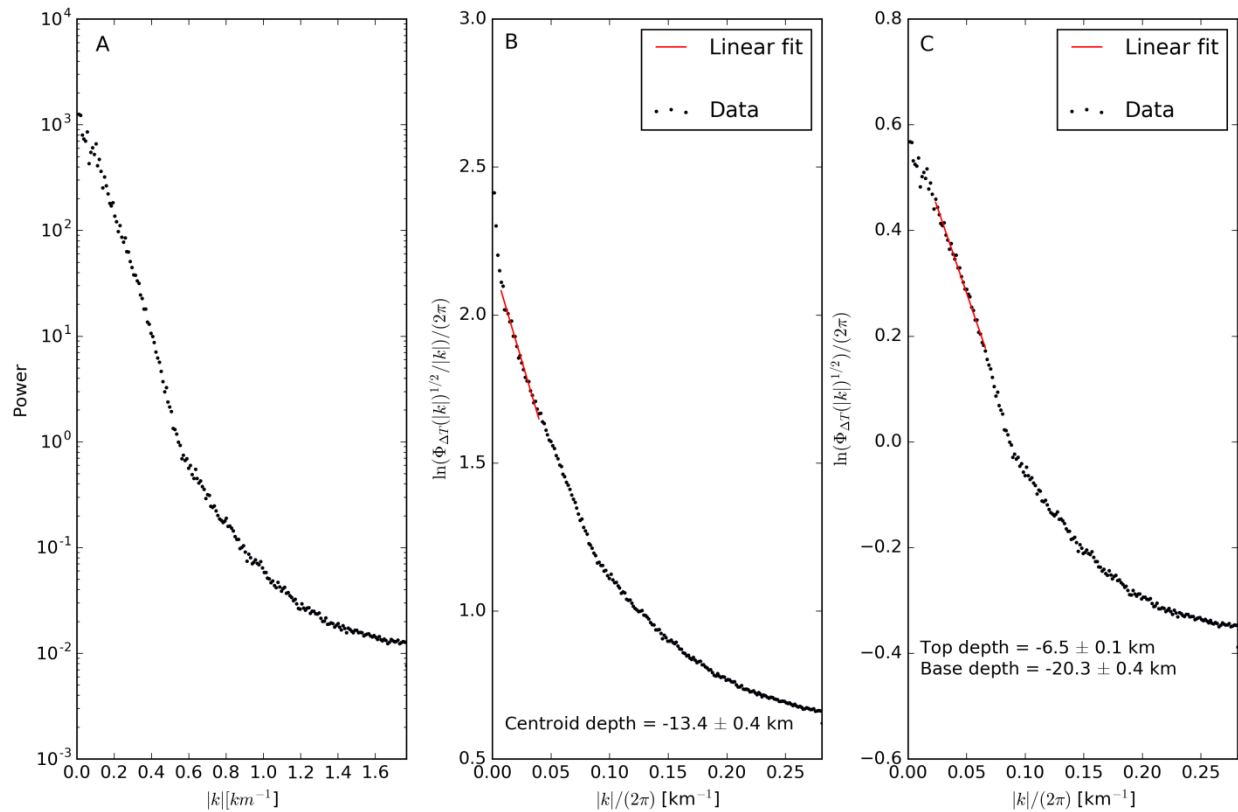


**Figure 4.** A) Plot of magnetic power spectrum vs. wavenumber for window 23. B) The depth to the centroid of the magnetic source ( $Z_o$ ) is calculated from the graph in the centre. C) The depth to the top of the magnetic source ( $Z_t$ ) is calculated from the graph on the right. The red lines in B) and C) show the slopes that were used in the  $Z_o$  and  $Z_t$  calculations. The depth to the base of the magnetic source ( $Z_b$  or the CPD) is calculated from:  $Z_b = 2Z_o - Z_t$ .

## 4. Results

The resulting CPD estimates (i.e.  $Z_b$  values) obtained for all 76 windows were plotted at the centre of each window and then contoured (Figure 5). Errors in the CPD values are estimated to be less than  $\pm 1.5$  km (~5-10% of the depth).

The Curie point depth estimates range from 18-36 km. These values are typical of continental cordillera (cf. Afghanistan CPD range is 16-40 km; Saibi et al., 2015). The deepest CPD values (30-36 km) are located in the northeast quadrant and along the south central edge of the study area. Shallower CPD estimates (18-24 km) occupy the southeast corner and much of the western half of the region studied (Figure 5). For comparison, typical CPD values for subduction zones and active volcanoes are commonly less than ~10 km (Tanaka et al., 1999; De Ritis et al., 2013). CPD values at this depth were not identified in the study area.

The CPD contours overlain on the magnetic data in the study area are shown in Figure 6. A complete list of the  $Z_t$ ,  $Z_o$ , and  $Z_b$  values are presented in Appendix 1. In the next section, the Curie point depth map generated for the pilot study area is interpreted in a general way in light of existing heat flow data, regional geology, and the locations of hot springs and Holocene volcanic centres.

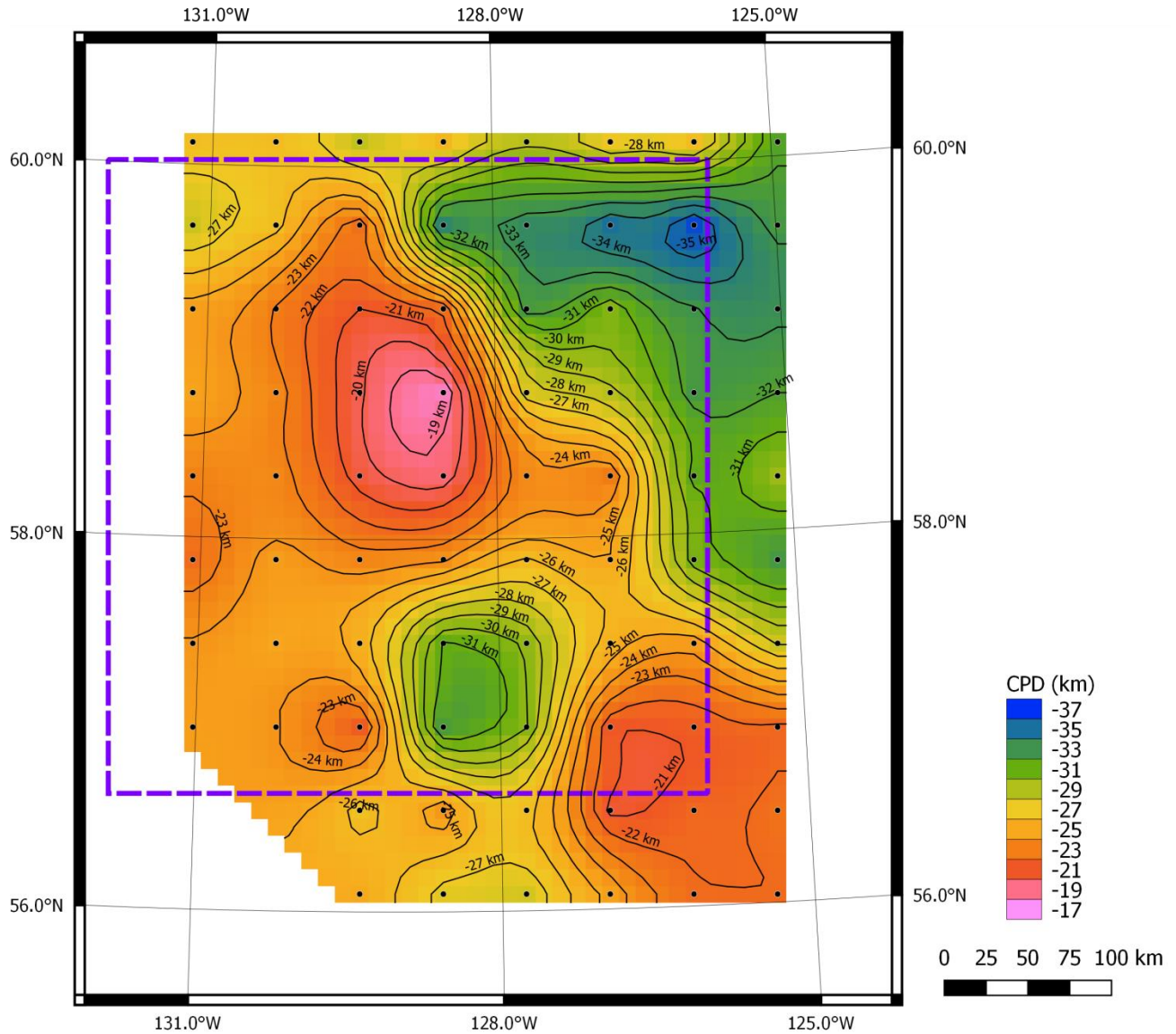


**Figure 5.** Curie point depth map for northwestern BC. The pilot study boundary is shown by the purple dashed line and window centres are shown as black dots. Warm and cool colours represent shallow and deep CPD estimates, respectively. Contour lines show CPD in units of kilometres below the surface. The CPD estimates do not extend to the western edge of the pilot study area due to a lack of magnetic data outside the study area in these regions.

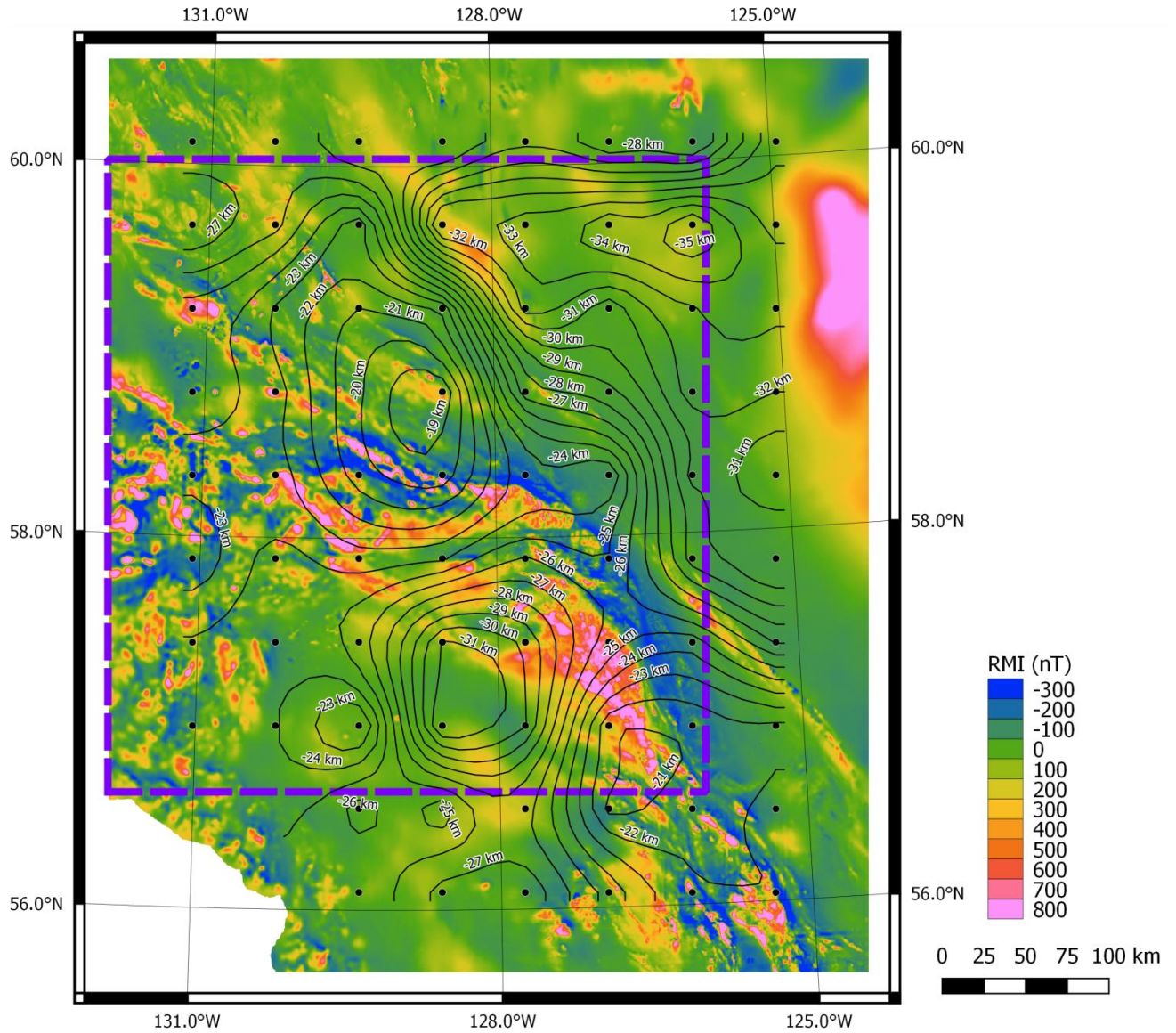


**Figure 6.** Curie point depth map for northwestern BC underlain by magnetic data. The pilot study boundary is shown by the purple dashed line and window centres are shown as black dots. Warm and cool colours represent magnetic highs and lows (in nT), respectively. Contour lines show CPD in units of kilometres below the surface.

## 5. Discussion

### *Comparison with Hot Springs and Volcanoes*

A comparison between the CPD estimates with the locations of hot springs and Holocene volcanoes is shown in Figure 7. Several hot springs located in the western portion of the study area coincide with relatively shallow CPD values (< 25 km). However, a number of hot springs also occur in the northeast corner of the study region and correlate with some of the deepest CPD encountered (> 30 km). Thus, a consistent correlation between shallow CPD values and hot springs is not evident.

Holocene volcanic centres are located near the western edge of the study area and coincide with relatively shallow CPD values (23-25 km). These volcanoes, however, do not correlate with the shallowest CPD value identified. The 19 km CPD contour near the center of the study area lies ~100 km from the nearest volcanic centre. One possible explanation for this shallow (19 km) CPD is intrusion of magma into the deep crust since this location does lie within the Northern Cordilleran Volcanic Province (Edwards and Russell, 1999).

### *Comparison with Heat Flow*

Several studies have shown a correlation between high heat flow measurements and shallow CPD (e.g. Okubo et al., 1985; Tanaka et al., 1999; Manea and Manea 2011; Hsieh et al., 2014). Figure 8 shows a map comparing heat flow data from wells with the calculated CPD from this study. Although the heat flow data are sparse, the general trend is for lower heat flow values in the east (42 – 70 mW/m<sup>2</sup>; just outside of the CPD study area) and higher heat flow in the west (65 – 118 mW/m<sup>2</sup>). The average heat flow for all of Canada is 64 +/- 16 mW/m<sup>2</sup> (Grasby et al., 2012). These general east-west trends in heat flow agree well with observed shallower CPD in the west and deeper CPD towards the east. Direct correlation of individual heat flow anomalies with peaks and troughs in CPD is difficult, primarily due to a lack of heat flow data points. For example, the 19 km shallow CPD contour in the centre of the study area and the 31 km

deep CPD in the south both lie in areas with no heat flow data. Indeed, there are only ~10 heat flow measurements within the boundary of the CPD study area.

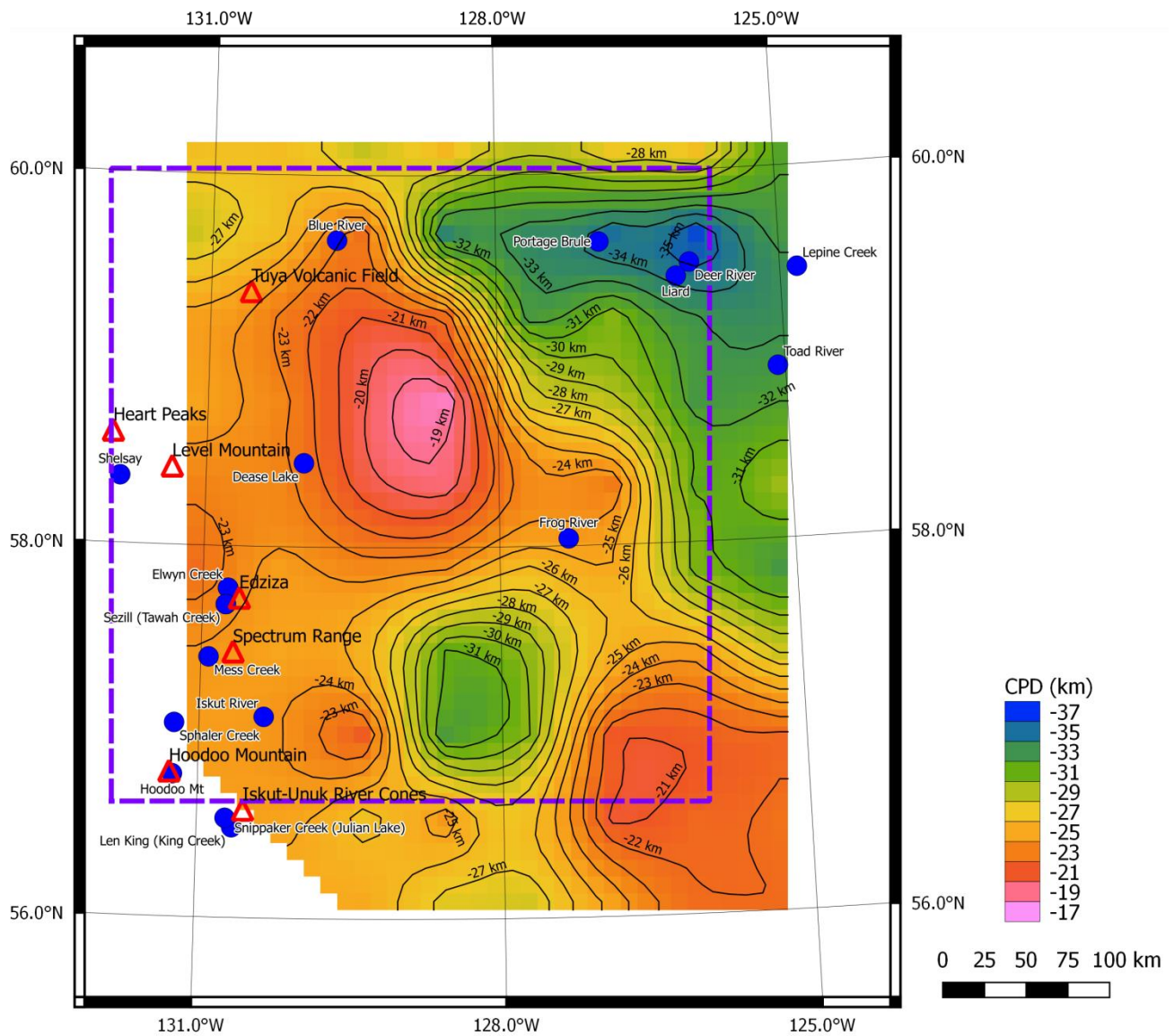


**Figure 7.** Comparison between the Curie point depth map for northwestern BC and the locations of hot springs (blue dots) and Holocene volcanic centres (red triangles). The pilot study boundary is shown by the purple dashed line.

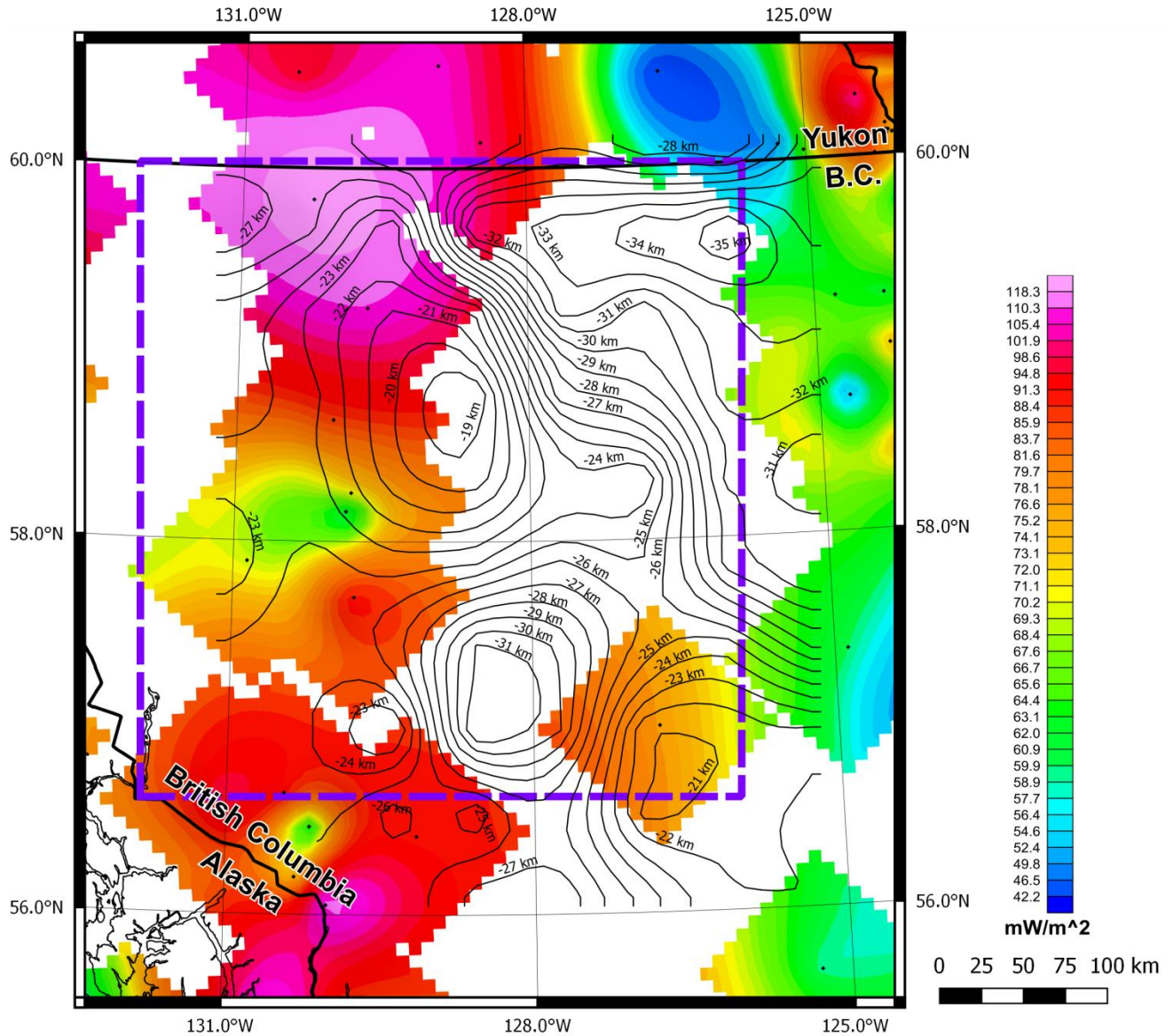


**Figure 8.** Comparison between the existing heat flow map for British Columbia and the Curie point depth map generated in this pilot study. The CPD contours are shown as black lines and labelled. Heat flow is shown in the background with warm and cool colours representing high and low heat flow respectively. Locations of heat flow data points are shown as small black diamonds. Heat flow map is from Geoscience BC (2016).

### *Comparison with Regional Geology and Major Faults*

The geology of northwestern British Columbia consists of a variety of accreted terranes that have amalgamated with the North American continental margin since the Mesozoic (Nelson and Colpron, 2007). The area covered by this study straddles the contact between Ancestral North America and the younger belts of the accreted Intermontane terranes (Figure 9). The northwest-trending Tintina Fault matches well with the boundary between deep CPD values to the east, associated with Ancestral North America, and shallower CPD values to the west. Curiously, two areas exhibiting shallow CPD values lie on top of major fault zones. For example, the shallow CPD (~19 km) located near the centre of the study area sits astride the northwest-trending, right lateral Teslin fault zone in a geologically complex area that includes the Cache Creek, Quesnellia, Cassiar, Slide Mountain, and Yukon-Tanana terranes (Figure 9). The shallow CPD (~21 km) located in the southeast corner of the study area coincides with the north-northwest-trending, right lateral Takla-Finlay-Ingenika fault system (Nelson and Colpron, 2007). Lastly, the deep CPD (~31 km) that sits in the south central portion of the study area occupies a region just west of the Teslin fault zone and within the Stikinia terrane, a Paleozoic-Mesozoic volcanic arc.

A detailed interpretation of the CPD results and their geological meaning with respect to the architecture of the Earth's crust in northwest BC is beyond the scope of this project. However, some possible explanations are presented here. First, the deep CPD values derived for the North American craton are not surprising. Cratonic rocks are old, have low thermal conductivity, limited heat generation potential, and generally have low heat flow. Second, relatively shallow CPD values associated with major fault zones could possibly be due to localized, fault-parallel extension that has thinned the crust in these areas to allow hotter material to rise to shallower depths. Alternatively, deep hydrothermal processes within these fault zones could potentially be destroying magnetite in the crust at depth thereby creating a shallower base of the magnetic source.

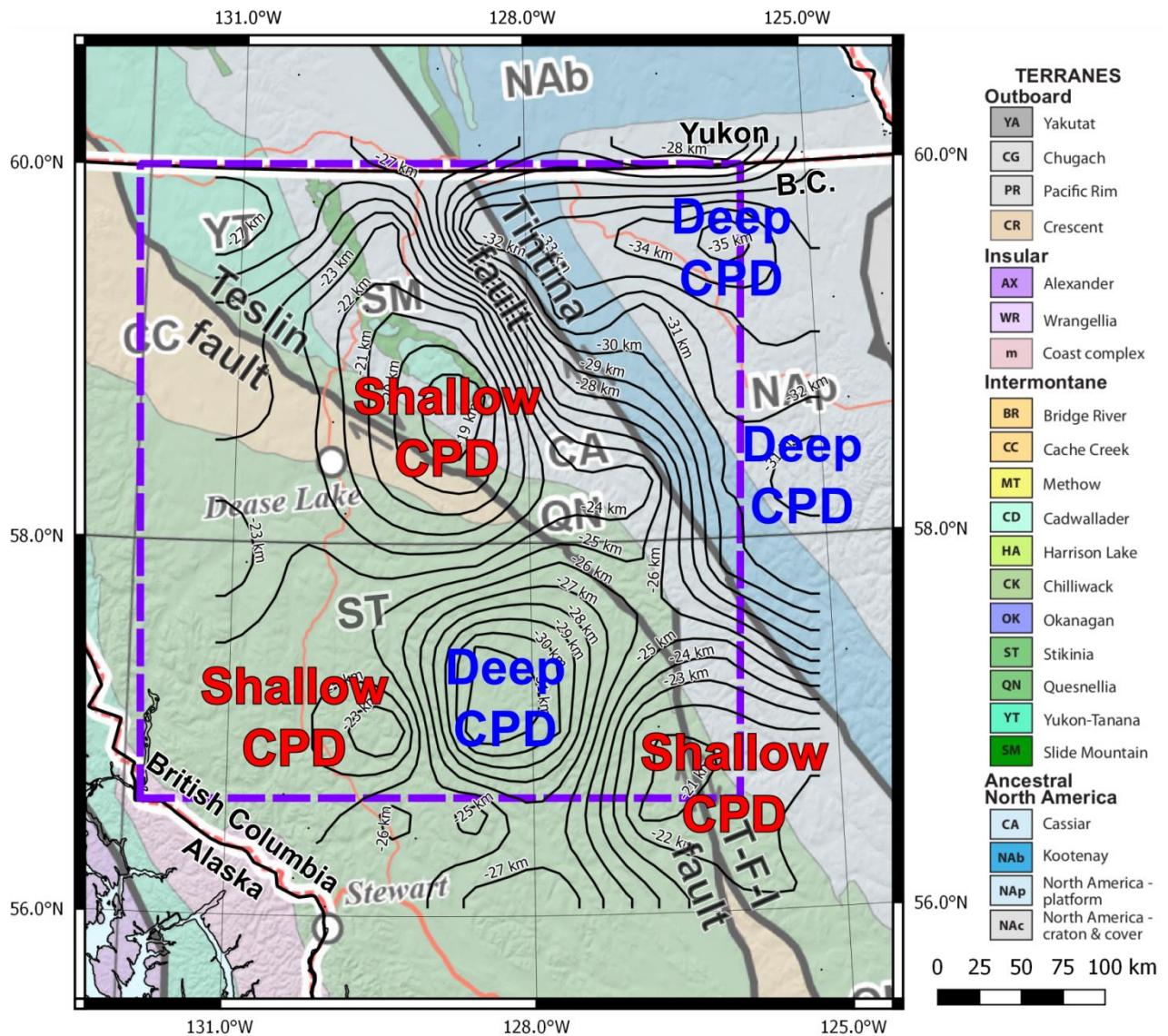


**Figure 9.** Comparison between the regional geologic terrane map for British Columbia (adapted from Colpron and Nelson, 2011) and the Curie point depth map generated in this pilot study. T-F-I fault stands for Takla-Finlay-Ingenika fault.

### *Implications for Geothermal Resource Exploration*

Simple calculations can convert the depth to the Curie point into average temperature gradient and heat flow estimates to help assess the geothermal energy potential of the area. To do so, we use the following equations (Tanaka et al, 1999; Turcotte and Schubert, 1982):

$$dT/dZ = 580 \text{ }^{\circ}\text{C} / Z_b \quad (1)$$

$$Q = k * dT/dZ \quad (2)$$

where  $dT/dZ$  is the temperature gradient in  $^{\circ}\text{C}/\text{km}$ ,  $Z_b$  is the magnetic source base depth (i.e. the Curie point depth) in km,  $Q$  is heat flow in  $\text{mW}/\text{m}^2$ , and  $k$  is thermal conductivity in  $\text{W}/\text{mK}$ . The calculated heat flow is critically dependent on the value chosen for thermal conductivity. As discussed in the previous section, the geology in the pilot study area is complex and a single assumed value for  $k$  assigned to the whole region is likely inappropriate. For demonstration purposes, however, we assume a thermal conductivity of  $3.2 \text{ W}/\text{mK}$  (a typical value for crystalline rocks; Grasby et al., 2012) to generate heat flow estimates for the area using this technique. A more rigorous approach (outside the scope of this study) would involve assigning specific thermal conductivity values to different geologic domains and then estimate heat flow from the CPD values. Assuming a uniform thermal conductivity of  $3.2 \text{ W}/\text{mK}$  generates heat flow estimates described below.

For the relatively deep ( $> 30 \text{ km}$ ) CPD values determined for the North American craton in the eastern portion of the study area, our calculations suggest that average temperature gradients in this area are likely to be  $< 20 \text{ }^{\circ}\text{C}/\text{km}$  with heat flow values  $< 60 \text{ mW}/\text{m}^2$ . These results suggest that this portion of the pilot study area may be less prospective for shallow, high temperature, electricity-grade geothermal resources. However, evidence for lower temperature, direct-use geothermal resources in the area is strong. For example, hot springs such as the Liard, Portage Brule, and Deer River with discharge temperatures of  $52$ ,  $44$ , and  $35 \text{ }^{\circ}\text{C}$ , respectively, (Geoscience BC, 2016) are present in this part of the study area. Despite the deep CPD, these hot springs reveal that lower temperature geothermal fluids are able to migrate to the surface.

In the western portion of the study area, where CPD values are shallower (i.e. 18 – 24 km), our calculations suggest that average temperature gradient can be expected to be 24 – 32 °C/km with heat flow values of 75 – 101 mW/m<sup>2</sup>. Such elevated heat flow values are typical of known geothermal regions such as the Great Basin in the western United States (Blackwell et al., 2011). As an example, the state of Nevada alone, located within the Great Basin, has over 600 MWe of installed geothermal electric capacity at ~17 power stations (Geothermal Energy Association, 2016). By analogy then, this portion of northwestern BC is likely prospective and geothermal exploration programs should focus on shallow CPD areas.

This brief thermal analysis presumes a linear temperature gradient from the surface to the Curie point depth (i.e. tens of kilometres), and does not preclude shallower zones (i.e. several kilometres) from having anomalous, elevated temperatures such as that found in some deep sedimentary basins.

## 6. Conclusions

In this pilot study, we calculated Curie point depth estimates across a ~350 km x ~350 km area of northwestern British Columbia using public domain magnetic survey data and the CPD analysis method of Tanaka et al. (1999). The depth estimates are assumed to correspond to a Curie temperature of 580 °C where magnetization disappears. Within the study area, the calculated CPD values have the range 18-36 km. In general, the deepest CPD values (> 30 km) lie in the northeastern part of the study area and coincide with the North American craton. The western boundary of this deep CPD zone corresponds with the Tintina fault zone. The southeast corner and most of the western half of the study area have relatively shallow CPD values of 18 – 24 km and are geologically represented by Intermontane terranes. Holocene volcanic centres of northwest BC are also located in the western portion of the study area. The CPD estimates under these volcanic centres (23 – 24 km), however, are much deeper than typical CPD values below active volcanoes (i.e. < 10 km). There appears to be no consistent correlation between CPD value and hot spring locations. Although heat flow data from existing wells are sparse, regions of higher heat flow in the study area generally correspond to zones with shallower CPD and vice versa. CPD data itself can also be used to calculate heat flow if we assume a value for the average thermal conductivity of the crust. With such an assumption, CPD values of 18 – 24 km in the study area correspond to heat flow values of 75 – 101 mW/m<sup>2</sup> which are in general agreement with the range of measured heat flow data in the western half and southeast corner of the study area. Such high heat flow values are typical of electricity-grade geothermal regions such as the Great Basin of the USA. Curie point depth mapping is a useful tool for regional assessment of deep crustal temperature across large areas. In this pilot study, we demonstrate that it is possible to estimate deep crustal temperatures and heat flow for all of BC using the CPD methodology described here. Nearly the entire province of British Columbia is covered by public domain magnetic survey data, therefore, CPD analysis can be applied province-wide. A CPD/heat flow map of British Columbia would complement the existing heat flow data for the province and could help guide future geothermal exploration programs towards more prospective areas.

## 7. Recommendations

- Perform Curie point depth mapping using public domain magnetic data across the entire province.
- Generate temperature gradient and heat flow maps for all of BC using CPD data.
- Use such maps in conjunction with existing heat flow data and other geoscience data to help guide electricity-grade and direct-use geothermal exploration programs.
- Collect additional airborne magnetic survey data to cover the portions of British Columbia where these data are lacking (i.e. the westernmost portions of the Cordillera; see Figure 1).

## 8. List of Deliverables

Filename	Description	Format
Curie Point Pilot Study report September 2016.pdf	This report	.pdf
Map 1 - CPD, hot springs, and volcanoes.pdf	Curie point depth contour map covering the pilot study area with Holocene volcanoes and hot springs for comparison	.pdf
Map 2 - CPD and Heat Flow.pdf	Curie point depth contour map covering the pilot study area with existing heat flow data for comparison	.pdf
Appendix 1 – CPD results.xlsx	Spreadsheet listing the X, Y, and depth locations of the calculated Curie point depth estimates	.xlsx
CPD contours.shp	Curie point depth map contour lines	.shp
CPD points.shp	Curie point depth data points located at the centres of the 100 km x 100 km calculation windows	.shp
CPD grid.tif	Curie point depth map shown as a grid of the datapoints	GeoTIFF
Residual Magnetic Intensity data.tif	Public domain magnetic data used in this study	GeoTIFF

## References

Aydin I, Karat HI, Koçak A (2005) Curie-point depth map of Turkey. *Geophysical Journal International*, v. 162, p. 633-640.

Bhattacharyya BK, Leu L-K (1975) Analysis of Magnetic Anomalies Over Yellowstone National Park: Mapping of Curie Point Isothermal Surface for Geothermal Reconnaissance. *Journal of Geophysical Research*, v. 80, no. 32, p. 4461-4465.

Bilim F, Akay T, Aydemir A, Kosaroglu S (2016) Curie point depth, heat-flow and radiogenic heat production deduced from the spectral analysis of the aeromagnetic data for geothermal investigation on the Menderes Massif and the Aegean Region, western Turkey. *Geothermics*, v. 60, p. 44-57.

Blackwell DD, Richards MC, Frone ZS, Batir JF, Williams MA, Ruzo AA, Dingwall RK (2011) SMU Geothermal Laboratory Heat Flow Map of the Conterminous United States, 2011. <http://www.smu.edu/geothermal>

Blakely RJ (1988) Curie Temperature Isotherm Analysis and Tectonic Implications of Aeromagnetic Data from Nevada. *Journal of Geophysical Research*, v. 93, No. B10, P. 11,817-11,832.

Bouligand C, Glen JMG, Blakely RJ (2009) Mapping Curie temperature depth in the western United States with a fractal model for crustal magnetization. *Journal of Geophysical Research*, v. 114, B11104, doi:10.1029/2009JB006494.

Colpron M, Nelson J (2011) A Digital Atlas of Terranes for the Northern Cordillera. Yukon Geological Survey and BC Geological Survey, [http://www.geology.gov.yk.ca/bedrock\\_terrane.html](http://www.geology.gov.yk.ca/bedrock_terrane.html)

Connard G, Couch R, Gemperle M (1983) Analysis of aeromagnetic measurements from the Cascade Range in central Oregon. *Geophysics*, v. 48, no. 3, p. 376-390.

DeRitis R, Ravat D, Ventura G, Chiappini M (2013) Curie isotherm depth from aeromagnetic data constraining shallow heat source depths in the central Aeolian Ridge (Southern Tyrrhenian Sea, Italy). *Bulletin of Volcanology*, 75:710, DOI 10.1007/s00445-013-0710-9.

Edwards BR, Russell JK (1999) Northern Cordilleran volcanic province: A northern Basin and Range? *Geology*, v. 27, no. 3, p. 243-246.

Edwards BR, Russell JK (2000) Distribution, nature, and origin of Neogene – Quaternary magmatism in the northern Cordilleran volcanic province, Canada. *GSA Bulletin*, v. 112, no. 8, p. 1280-1295.

Espinosa-Cardena JM, Campos-Enriquez JO (2008) Curie point depth from spectral analysis of aeromagnetic data from Cerro Prieto geothermal area, Baja California, México. *Journal of Volcanology and Geothermal Research*, v. 176, p. 601-609.

Geothermal Energy Association (2016) 2016 Annual U.S. & Global Geothermal Power Production Report. 36 pages, <http://geo-energy.org/reports.aspx>

Geoscience BC (2016) Direct-use Geothermal Resources in British Columbia. Report 2016-07, <http://www.geosciencebc.com/s/Report2016-07.asp>

Grasby SE, Allen DM, Bell S, Chen Z, Ferguson G, Jessop A, Kelman M, Ko M, Majorowicz J, Moore M, Raymond J, Therrien R (2012) Geothermal Energy Resource Potential of Canada. Geological Survey of Canada, Open File 6914, 322 pages.

Hsieh H-H, Chen C-H, Lin P-Y, Yen H-Y (2014) Curie point depth from spectral analysis of magnetic data in Taiwan. *Journal of Asian Earth Sciences*, v. 90, p. 26-33.

Manea M, Manea VC (2011) Curie Point Depth Estimates and Correlation with Subduction in Mexico. *Pure & Applied Geophysics*, v. 168, p. 1489-1499.

Nelson J, Colpron M (2007) Tectonics and metallogeny of the British Columbia, Yukon and Alaskan Cordillera, 1.8 Ga to the present. In: Goodfellow WD, ed. *Mineral Deposits of Canada: A Synthesis of Major Deposit-Types, District Metallogeny, the Evolution of Geological Provinces, and Exploration Methods*, Geological Association of Canada, Mineral Deposits Division, Special Publication No. 5, p. 755-791.

Okubo Y, Graf RJ, Hansen RO, Ogawa K, Tsu H (1985) Curie point depths of the island of Kyushu and surrounding areas, Japan. *Geophysics*, v. 53, no. 3, p. 481-494.

Okubo Y, Tsu H, Ogawa K (1989) Estimation of Curie point temperature and geothermal structure of island arcs of Japan. *Tectonophysics*, v. 159, p. 279-290.

Ravat D, Pignatelli A, Nicolosi I, Chiappini M (2007) A study of spectral methods of estimating the depth to the bottom of magnetic sources from near-surface magnetic anomaly data. *Geophysical Journal International*, v. 169, p. 421-434.

Saibi H, Aboud E, Azizi M (2015) Curie Point Depth Map for Western Afghanistan Deduced from the Analysis of Aeromagnetic Data. *Proceedings World Geothermal Congress, Melbourne, Australia, 19-25 April, 12 pages.*

Shuey RT, Schellinger DK, Tripp AC, Alley LB (1977) Curie depth determination from aeromagnetic spectra. *Geophysical Journal of the Royal Astronomical Society*, v. 50, p. 75-101.

Smithsonian Institution Global Volcanism Program (2016) Google Earth placemarks. <http://volcano.si.edu/>

Spector A, Grant FS (1970) Statistical Models for Interpreting Aeromagnetic Data. *Geophysics*, v. 35, no.2, p. 293-302.

Tanaka A, Okubo Y, Matsubayashi O (1999) Curie point depth based on spectrum analysis of the magnetic anomaly data in East and Southeast Asia. *Tectonophysics*, v. 306, p. 461-470.

Turcotte DL, Schubert G, (1982) *Geodynamics. Applications of Continuum Physics to Geologic Problems.* Wiley, New York, 450 pp.

Vacquier V, Affleck J (1941) A computation of the average depth to the bottom of the earth's magnetic crust, based on a statistical study of local magnetic anomalies. *Transactions of the American Geophysical Union, 22<sup>nd</sup> Annual Meeting, 446-450.*

## Appendix 1: List of $Z_o$ , $Z_t$ , and $Z_b$ values

Window	Location (UTM NAD83 zone 9)		Centroid depth $Z_o$ (km)	Centroid depth error (km)	Top depth $Z_t$ (km)	Top depth error (km)	Base depth $Z_b$ (km)	Base depth error (km)
	Easting (m)	Northing (m)						
1	376729	6666579	-15.6	0.6	-4.8	0.2	-26.3	0.7
2	426525	6666579	-15.5	0.7	-4.8	0.1	-26.2	0.7
3	476604	6666579	-16.1	0.7	-3.8	0.2	-28.4	0.8
4	526684	6666579	-15.1	0.9	-4.3	0.2	-25.9	0.9
5	576480	6666579	-16.8	0.8	-4.9	0.2	-28.7	0.9
6	626559	6666579	-16.8	1	-6.9	0.2	-26.8	1
7	676639	6666579	-16.7	0.8	-7	0.2	-26.3	0.8
8	726718	6666579	-21.1	0.7	-10.4	0.3	-31.8	0.8
11	376729	6616785	-16.6	0.6	-5.1	0.2	-28.1	0.7
12	426525	6616785	-15.5	0.9	-4.6	0.2	-26.4	0.9
13	476604	6616785	-13.2	0.8	-4	0.2	-22.3	0.8
14	526684	6616785	-20.2	1.2	-6.6	0.2	-33.8	1.2
15	576480	6616785	-20.2	1.1	-6.9	0.2	-33.5	1.1
16	626559	6616785	-21.5	0.9	-8.2	0.4	-34.9	1
17	676639	6616785	-23.8	0.5	-11.5	0.4	-36.2	0.7
18	726718	6616785	-23.8	0.4	-14.9	1	-32.6	1.1
21	376729	6566709	-15.3	0.6	-6	0.2	-24.6	0.6
22	426525	6566709	-14.4	0.7	-6	0.1	-22.9	0.7
23	476604	6566709	-13.7	0.4	-6.5	0.1	-21	0.4
24	526684	6566709	-15.4	0.8	-8.6	0.2	-22.2	0.9
25	576480	6566709	-20	0.9	-7.5	0.2	-32.5	0.9
26	626559	6566709	-19.2	0.7	-8.2	0.2	-30.2	0.7
27	676639	6566709	-22.5	0.8	-12.2	0.3	-32.9	0.9
28	726718	6566709	-24.2	0.3	-15.1	1.1	-33.2	1.1
31	376729	6516633	-16.2	0.6	-7.6	0.2	-24.8	0.6
32	426525	6516633	-15.7	0.6	-7.8	0.2	-23.5	0.6
33	476604	6516633	-15.6	0.5	-11	0.2	-20.2	0.5
34	526684	6516633	-14.4	0.5	-10.8	0.2	-18	0.6
35	576480	6516633	-17.6	0.7	-7.6	0.1	-27.6	0.7
36	626559	6516633	-18	0.7	-7.2	0.1	-28.7	0.7
37	676639	6516633	-22.2	1	-11.8	0.6	-32.6	1.2
38	726718	6516633	-23.7	0.4	-15.3	1.2	-32	1.3
41	376729	6466839	-17	0.4	-10.8	0.2	-23.2	0.4
42	426525	6466839	-17	0.4	-10.6	0.2	-23.5	0.4
43	476604	6466839	-16.1	0.5	-11.8	0.2	-20.5	0.5
44	526684	6466839	-14.9	0.5	-10.4	0.3	-19.4	0.6
45	576480	6466839	-15	0.8	-6.4	0.2	-23.6	0.8
46	626559	6466839	-14	0.9	-5.1	0.2	-22.9	0.9
47	676639	6466839	-19	1	-6.6	0.2	-31.4	1
48	726718	6466839	-22.6	0.7	-15.7	1.3	-29.5	1.5

## Appendix 1 continued: List of $Z_o$ , $Z_t$ , and $Z_b$ values

Window	Location (UTM NAD83 zone 9)		Centroid depth $Z_o$ (km)	Centroid depth error (km)	Top depth $Z_t$ (km)	Top depth error (km)	Base depth $Z_b$ (km)	Base depth error (km)
	Easting (m)	Northing (m)						
51	376729	6416763	-17.1	0.4	-12.1	0.2	-22.1	0.5
52	426525	6416763	-17.6	0.4	-10.8	0.1	-24.5	0.5
53	476604	6416763	-17.1	0.5	-10.8	0.2	-23.4	0.5
54	526684	6416763	-16.5	0.5	-9.2	0.3	-23.8	0.6
55	576480	6416763	-15.9	0.7	-5.7	0.2	-26.1	0.7
56	626559	6416763	-14.9	0.8	-4.8	0.2	-25	0.9
57	676639	6416763	-17.9	0.8	-5.3	0.2	-30.5	0.9
58	726718	6416763	-19.3	0.6	-6	0.3	-32.6	0.7
61	376729	6366686	-17.5	0.5	-10.9	0.2	-24.1	0.5
62	426525	6366686	-17.4	0.7	-9.9	0.3	-24.9	0.8
63	476604	6366686	-17.6	0.8	-9.8	0.3	-25.5	0.9
64	526684	6366686	-19.2	0.9	-7.3	0.3	-31.1	0.9
65	576480	6366686	-17	0.8	-4.3	0.2	-29.8	0.8
66	626559	6366686	-15.1	0.8	-4.6	0.2	-25.6	0.8
67	676639	6366686	-14.8	0.8	-5.2	0.2	-24.4	0.8
68	726718	6366686	-16.8	0.7	-5.5	0.3	-28.1	0.7
71	376729	6316610	-17.6	0.5	-10.6	0.5	-24.5	0.7
72	426525	6316610	-17.7	0.6	-11.3	0.2	-24.1	0.7
73	476604	6316610	-14.9	0.7	-8.5	0.1	-21.3	0.7
74	526684	6316610	-22.2	0.8	-12.2	0.2	-32.3	0.9
75	576480	6316610	-17.3	0.9	-4.5	0.2	-30.1	0.9
76	626559	6316610	-13.2	0.6	-5.3	0.2	-21.1	0.7
77	676639	6316610	-13.3	0.6	-5.3	0.2	-21.3	0.6
78	726718	6316610	-13.5	0.5	-5.2	0.2	-21.8	0.6
83	476604	6266817	-18	0.7	-9.4	0.3	-26.5	0.7
84	526684	6266817	-18.1	0.8	-12	0.4	-24.2	0.9
85	576480	6266817	-16.4	0.8	-6.4	0.2	-26.4	0.8
86	626559	6266817	-13.1	0.5	-5.5	0.2	-20.7	0.5
87	676639	6266817	-13.7	0.4	-5.5	0.2	-21.9	0.4
88	726718	6266817	-14.1	0.4	-5.7	0.2	-22.4	0.5
93	476604	6216740	-18.1	0.5	-11	0.3	-25.1	0.6
94	526684	6216740	-19.8	0.7	-12.2	0.4	-27.4	0.8
95	576480	6216740	-16.4	0.8	-4.8	0.2	-27.9	0.8
96	626559	6216740	-14.6	0.8	-4.5	0.2	-24.7	0.8
97	676639	6216740	-13.6	0.5	-5.2	0.1	-22.1	0.5
98	726718	6216740	-13.5	0.5	-5	0.1	-22	0.5